

# Liouvillian topology and non-reciprocal dynamics in open Floquet chains

Florian Koch,<sup>1,2</sup> Yu-Min Hu,<sup>1</sup> and Jan Carl Budich<sup>1,2,\*</sup>

<sup>1</sup>Max Planck Institute for the Physics of Complex Systems, Nöthnitzer Str. 38, 01187 Dresden, Germany

<sup>2</sup>Institute of Theoretical Physics, Technische Universität Dresden and

Würzburg-Dresden Cluster of Excellence ct.qmat, 01062 Dresden, Germany

(Dated: November 20, 2025)

Open quantum systems far from thermal equilibrium can exhibit remarkable physical phenomena including topological properties without a direct equilibrium counterpart. Along these lines, in periodically driven dissipative systems within the effective non-Hermitian (NH) Hamiltonian approximation spectral winding numbers have been linked to intriguing nonreciprocal transport properties. Here, going beyond an NH Hamiltonian description, we introduce and study a microscopic lattice model of a driven open quantum system described by a Markovian quantum master equation, which exhibits the mentioned spectral winding within a NH approximation. By encompassing quantum jump processes in the topological analysis, we uncover a distinct *jump-induced* topological phase, which qualitatively corresponds to the richer non-reciprocal transport properties of the fully quantum model. In addition, we find that the NH skin effect, i.e. the accumulation of a macroscopic number of eigenstates at one end of the system, is already visible in the transient dynamics even for systems with periodic boundary conditions. Our results exemplify the subtle correspondence between NH topological properties and physical manifestations of Liouvillian topological properties in open quantum systems, thus providing a theoretical framework towards understanding unidirectional transport in quantum dissipative Floquet dynamics.

## I. INTRODUCTION

Exploring the role of topology in non-equilibrium dynamics has led to the discovery of numerous intriguing topological phenomena, some of which do not have a direct equilibrium counterpart [1–10]. Two interdisciplinary frontiers of current research along these lines are provided by the study of periodically driven (Floquet) systems [11–17] and the effective non-Hermitian (NH) Hamiltonian approach to dissipative dynamics [18–24]. Bridging the two aforementioned concepts, topological properties of effective NH Floquet Hamiltonians describing driven dissipative systems have recently been investigated [25–34]. This raises the natural question as to what extent these findings may be transferred from the effective NH Hamiltonian level to a fully quantum mechanical description in the framework of quantum master equations [35–38]. Motivated by preliminary insights into the relation of NH and Liouvillian topology [32, 39–43], the objective of our present work is to address this question both at the abstract level of defining the quantum dissipative counterpart of NH Floquet topological invariants and at the practical level of predicting observable physical phenomena relating to them.

Below, we introduce a microscopic quantum model for a dissipative one-dimensional (1D) Floquet chain by adding on-site spin relaxation to a helical Floquet channel (see Fig. 1 for an illustration), which is characterized by the locking of spin and direction of motion [40, 44]. When employing an effective NH Hamiltonian approximation, the classical counterpart of our model realizes a NH topological Floquet phase with complex spectral winding of the

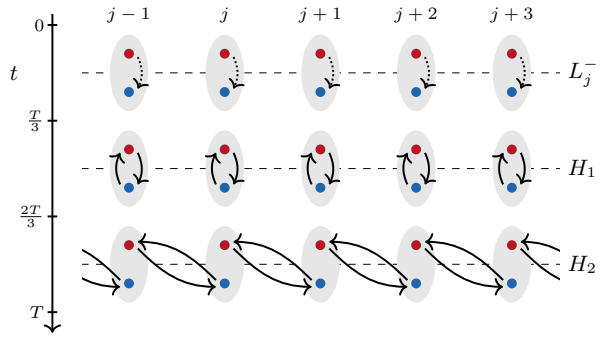


Figure 1. Schematic illustration of the dissipative Floquet chain of spin- $\frac{1}{2}$  fermions over one Floquet period  $T$ . Each site  $j$  (grey circle) hosts spin-up (red) and spin-down (blue) states. Dotted arrows denote spontaneous decay via  $L_j^-(t) = \sqrt{\gamma(t)} \sigma_j^-$ , while solid arrows indicate coherent dynamics generated by the Hamiltonians  $H_1$  and  $H_2$ . This serves as the minimal model studied here, alongside more experimentally realistic variants discussed in the text.

Floquet-operator in the sense of Ref. [27]. Interestingly, we find that considering the full Liouvillian dynamics governed by the Lindblad master equation including quantum jump processes significantly enriches the phenomenology. In particular, the preferred direction of non-reciprocal transport [45, 46], which arises from the spin-momentum locking of the clean model due to dissipation, becomes tunable with basic model parameters. This finding is in qualitative agreement with a sign change of a Liouvillian winding number that we construct as a topological invariant for the quantum model and which is absent in the approximate NH description. Moreover, we demonstrate how the NH skin effect, i.e. the accumulation of

\* jcbudich@pks.mpg.de

a macroscopic number of eigenstates at one end of a 1D chain with open boundary conditions [24, 47–51], leaves clear fingerprints in the (sub-extensive) transient dynamics even in the case of periodic boundary conditions. Our results are corroborated by the numerically exact solution of the quantum master equation.

The remainder of this article is structured as follows. In Sec. II, we introduce the quantum model as a dissipative extension of the helical Floquet model of Ref. [40], where the dissipation is engineered to act only during an additional Floquet waiting phase, serving as a toy model to illustrate the key concepts in contrast to the physical dissipation treated later. In Sec. III, we investigate the effective non-Hermitian approximation, and in Sec. IV we turn to the full dissipative quantum dynamics governed by the Lindblad master equation. Each of these sections is structured into three parts: (i) the topological properties, (ii) transport and topology under periodic boundary conditions, and (iii) the behavior under open boundary conditions, including the non-Hermitian skin effect. Finally, in Sec. V, we propose an experimentally feasible implementation that incorporates dissipation (spontaneous decay and dephasing) throughout the dynamics.

## II. MODEL

We consider a periodically driven one-dimensional lattice model of spin-1/2 fermions with dissipation, whose dynamics is governed by the time-dependent Lindblad master equation [52, 53]

$$\frac{d}{dt}\rho = \mathcal{L}(t)[\rho] = -i[H_S(t), \rho] + \sum_{\kappa} \gamma_{\kappa}(t) \mathcal{D}_{L_{\kappa}}[\rho] \quad (1)$$

where  $\rho$  is the density matrix,  $H_S(t)$  is the periodically driven Hamiltonian,  $\gamma_{\kappa}(t)$  are time-periodic dissipation rates and  $\mathcal{D}_L[\rho] = L\rho L^{\dagger} - \frac{1}{2}\{L^{\dagger}L, \rho\}$  is the Lindblad dissipator for the jump operators  $L_{\kappa}$ . As introduced in the following, the Floquet driving is implemented through a linearly segmented three-phase cycle of total duration  $T$ , such that

$$H_S(t+T) = H_S(t), \quad \gamma_{\kappa}(t+T) = \gamma_{\kappa}(t). \quad (2)$$

The spinor operator  $\psi_j = (\psi_{j\downarrow}, \psi_{j\uparrow})$  annihilates a fermion on the lattice with unit lattice constant on the  $j$ th site. With the standard Pauli matrices  $\sigma_{x,y,z}$  [54] and the spin-flip operators  $\sigma_{\pm} = \frac{1}{2}(\sigma_x \pm i\sigma_y)$ , we define the Hamiltonians  $H_1 = \beta \sum_{j=1}^L \psi_j^{\dagger} \sigma_x \psi_j$  and  $H_2 = -\alpha \sum_{j=1}^L \psi_j^{\dagger} \sigma_z \psi_{j+1} + \text{h.c.}$

We also consider the spontaneous decay of the spin that acts locally on each site  $j$ , which is described by the jump operators [55, 56]

$$L_j^- = \psi_j^{\dagger} \sigma_- \psi_j. \quad (3)$$

We further assume that the dissipation rates are equal on each site, i.e.  $\forall j : \gamma_j(t) = \gamma(t)$ . The time dependencies

of the Hamiltonian and the dissipation rate can then be written as

$$H_S(t) = \begin{cases} 0 & \text{if } t \in [0, \frac{T}{3}), \\ H_1 & \text{if } t \in [\frac{T}{3}, \frac{2T}{3}), \\ H_2 & \text{if } t \in [\frac{2T}{3}, T). \end{cases} \quad (4)$$

$$\gamma(t) = \begin{cases} \gamma & \text{if } t \in [0, \frac{T}{3}), \\ 0 & \text{if } t \in [\frac{T}{3}, T). \end{cases} \quad (5)$$

In Sec. V, we extend this model to a more realistic setting by including dephasing and applying dissipation during the full time evolution. Throughout the manuscript, we set the parameter  $\alpha = \frac{3\pi}{2T}$ . Further, we denote site indices by  $m, m', n, n', j$  and spin indices by  $s, s', r, r'$ . For brevity and readability, we use the shorthand  $\sum_{s \in \{\downarrow, \uparrow\}} \rightarrow \sum_s$  and  $\sum_{j=1}^L \rightarrow \sum_j$  (and similarly for the other indices introduced above).

Defining the particle number operator  $N = \sum_{j,s} \psi_{js}^{\dagger} \psi_{js}$  and the translation operator  $T_a = \sum_{j,s} \psi_{j+a,s}^{\dagger} \psi_{j,s}$ , we find that at all times  $t$ , the dynamics conserve particle number,

$$[H_S(t), N] = [L_j^-, N] = 0, \quad (6)$$

and is translation invariant (assuming periodic boundaries  $\psi_{L+a,\sigma} = \psi_{a,\sigma}$ )

$$T_1 \mathcal{L}(t)[\rho] T_1^{\dagger} = \mathcal{L}(t)[T_1 \rho T_1^{\dagger}]. \quad (7)$$

We stress that our present discussion focuses on the single-particle sector of the model. The corresponding single-particle states are defined by  $|j, s\rangle = \psi_{js}^{\dagger} |\text{vac}\rangle$ . It follows that the Liouvillian propagator  $\mathcal{U}(t_0, t) = \mathcal{T} \exp(\int_{t_0}^t \mathcal{L}(t') dt')$  must also be number-conserving and translation-invariant. We define the Floquet-Liouvillian propagator

$$\mathcal{F} = \mathcal{U}(T, 0) \quad (8)$$

which describes the time-evolution over a single Floquet period and thus governs the stroboscopic dynamics.

In the limit of zero dissipation, this model recovers the Helical Floquet model of Ref. [40]. Since the Hamiltonians are translational invariant, we can apply a Fourier transform  $|k, s\rangle = \frac{1}{\sqrt{L}} \sum_j e^{-ijk} |j, s\rangle$  and write the unitary time-evolution operator  $U^k(T, 0) = \exp(-iH_2^k T/3) \exp(-iH_1^k T/3)$  of a single Floquet phase  $T$  in lattice momentum space, where  $H_1^k = \beta \sigma_x$  and  $H_2^k = -\alpha [\cos(k) \sigma_x - \sin(k) \sigma_y]$  are the Bloch Hamiltonians corresponding to  $H_1$  and  $H_2$ , respectively. A particularly interesting special case occurs for  $\frac{\alpha T}{3} = \frac{\beta T}{3} = \frac{\pi}{2}$ , where  $U^k(T, 0) = e^{ik\sigma_z}$  realizes perfect helical spin transport [40], i.e. as  $k$  varies from  $-\pi$  to  $+\pi$ , the two eigenvalue branches wind in opposite direction – one clockwise and the other counterclockwise – around the unit circle. In the following, we address an important question: How

does the dissipation alter the transport in the original closed system. As a first step, we will take a look at the effective non-Hermitian approximation where a theory of topological transport has been developed in Ref. [27].

### III. EFFECTIVE NON-HERMITIAN APPROXIMATION

The effective non-Hermitian Hamiltonian is defined as [57–60]

$$H_{\text{NH}} = H_S - \frac{i}{2} \sum_{\kappa} \gamma_{\kappa} L_{\kappa}^{\dagger} L_{\kappa}. \quad (9)$$

By neglecting the quantum jumps ( $\propto L_{\kappa} \rho L_{\kappa}^{\dagger}$ ), the Lindblad master equation reduces to a von-Neumann-like equation [61]

$$\frac{d}{dt} \rho = -i(H_{\text{NH}} \rho - \rho H_{\text{NH}}^{\dagger}) \quad (10)$$

which is solved by  $\rho(t) = U_{\text{NH}}(t, t_0) \rho(t_0) U_{\text{NH}}^{\dagger}(t, t_0)$  with  $U_{\text{NH}}(t, t_0) = \mathcal{T} \exp(-i \int_{t_0}^t H_{\text{NH}}(\tau) d\tau)$ . This shows that under this time-evolution, a pure state remains pure, i.e.  $|\varphi(t)\rangle = U_{\text{NH}}(t, t_0) |\varphi(t_0)\rangle$ . Similar to the Lindbladian case, we define the one-period Floquet propagator  $F = U_{\text{NH}}(T, 0)$ , which controls the stroboscopic dynamics. However, since  $U_{\text{NH}}(t, t_0)$  is non-unitary, the norm  $\|\varphi(t)\|$  is not conserved, reflecting gain and loss. In open quantum systems, this change can be interpreted as the probability of a quantum jump occurring [60]. Consequently, a substantial deviation of  $\langle \varphi(t) | \varphi(t) \rangle$  from unity signals that quantum jumps become relevant.

We note that a complementary interpretation of an effective NH Hamiltonian approximation is to neglect quantum noise in a quantum Langevin equation [41, 55, 56]. In this context, which is familiar in photonic systems, the NH Hamiltonian is thus tantamount to a classical limit.

In this section, we focus on the non-unitary dynamics of pure states which is in principle applicable to either of the aforementioned interpretations of NH Hamiltonians, aiming at discussing the topology of non-Hermitian Floquet chains. A quantum treatment based on the full Lindblad master equation will be elaborated in the next section.

#### A. Topology of non-Hermitian Floquet chains

In Ref. [27] a topological winding number for non-Hermitian Floquet chains has been introduced and linked to transport properties of the system. Here, a short review of this theory is given, adapting it to the NH (or classical) limit of our model with spin in addition to spatial degrees of freedom.

Let the stroboscopic dynamics of the translation-invariant system be described by the non-unitary Floquet operator

$$F = \sum_{s,s'} \int_{-\pi}^{\pi} F^{ss'}(k) |k, s\rangle \langle k, s'| dk, \quad (11)$$

the spectrum of which is restricted to the punctured complex plane  $\mathbb{C} \setminus \{0\}$  due to the invertibility  $F(t)^{-1} = F(-t)$  of the propagator. The individual eigenvalues  $\xi_a(k) = e^{-i\epsilon_a(k)}$  of  $F(k)$  therefore must form closed loops in  $\mathbb{C} \setminus \{0\}$  due to the periodicity of the quasienergies  $\epsilon_a(k)$ . Considering the origin of the complex plane as the natural point gap for the Floquet operator, eigenvalues winding around it create a non-trivial topology. To this end, a winding number  $W(\Gamma)$  for the dominant quasienergy bands is defined as

$$W(\Gamma) = \frac{i}{2\pi} \sum_{e^{\Gamma} < |\xi_a|} \int_{-\pi}^{\pi} \xi_a(k)^{-1} \partial_k \xi_a(k) dk \quad (12)$$

where  $\Gamma$  defines an imaginary gap  $i\Gamma$  that separates the eigenvalues and the condition  $e^{\Gamma} < |\xi_a(k)|$  picks out the dominant quasienergy bands of the system. Figure 2(d) shows the eigenvalues for two parameter sets, with blue indicating topologically trivial and red indicating non-trivial phases, where an imaginary gap is given by the dashed red line.

This winding number can be related to the mean transferred charge  $\bar{C} = \bar{C}_n(1)$ , which is defined as the average propagation distance

$$\bar{C}_n(p) = \frac{1}{2p} \sum_s \langle \varphi_{ns}(pT) | x - n | \varphi_{ns}(pT) \rangle \quad (13)$$

where  $|\varphi_{ns}(pT)\rangle = F^p |n, s\rangle$  is the state after  $p$  Floquet cycles,  $x = \sum_{j,s} j |j, s\rangle \langle j, s|$  is the position operator and  $n$  is the initial site index, which is irrelevant due to translation invariance. The prefactor  $\frac{1}{2p}$  reflects averaging over  $p$  Floquet cycles and the two spin degrees of freedom. Introducing the spin-averaged initial density matrix  $\rho_n(0) = \frac{1}{2} \sum_s |n, s\rangle \langle n, s|$ , which describes an unpolarized fermion on site  $n$ , we can write the average propagation distance compactly as  $\bar{C}_n(p) = \frac{1}{p} \langle x - n | \rho_n(pT) \rangle$ , where  $\rho_n(pT) = F^p \rho_n(0) (F^{\dagger})^p$ . Note that the time-evolved states must not be normalized because of the non-Hermiticity and thus, the propagation distance is weighted by  $\text{Tr}[\rho_n(pT)] \neq 1$ .

In the thermodynamic limit  $L \rightarrow \infty$  and with periodic boundaries, the mean transferred charge  $\bar{C}$  can be expressed in the lattice momentum space as

$$\bar{C} = \frac{i}{4\pi} \int_0^{2\pi} \text{Tr}_S [F^{\dagger}(k) \partial_k F(k)] dk \quad (14)$$

where  $\text{Tr}_S A = \sum_s A_{ss}$  denotes the trace over the spin degrees of freedom of the Fourier-transformed operator.

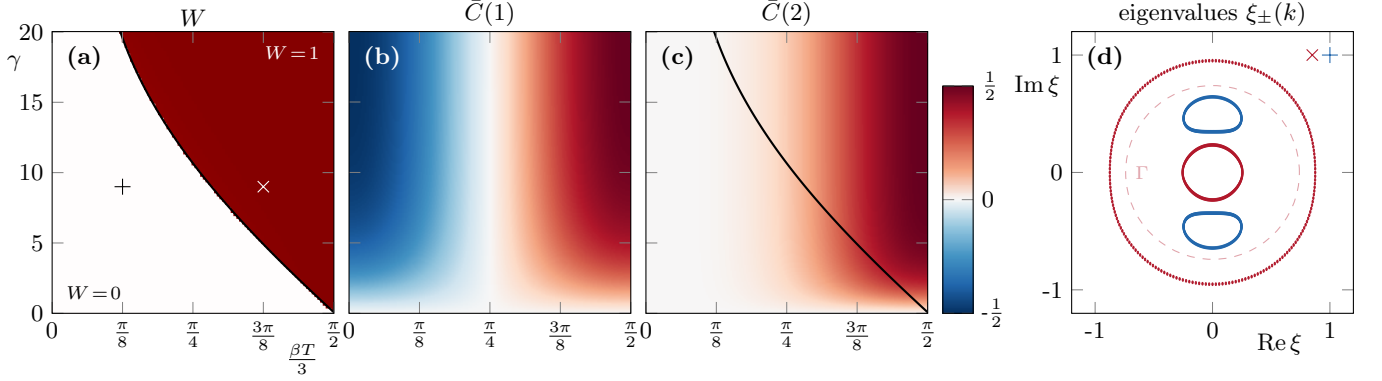


Figure 2. (a) Topological winding number as a function of the parameters  $\beta$  and  $\gamma$ . The parameter sets  $(\frac{\beta T}{3}, \gamma) = (\frac{\pi}{8}, 9)$  and  $(\frac{3\pi}{8}, 9)$  are highlighted, with their corresponding eigenvalues shown in (d). (b,c) Mean transferred charge  $\bar{C}(p)$  after  $p = 1$  (b) and  $p = 2$  (c) Floquet cycles, plotted versus  $\beta$  and  $\gamma$ . (d) Spectral distribution of the non-unitary Floquet propagator  $F$  in the punctured complex plane; the dashed red circle shows a choice of an imaginary gap  $\Gamma$ , with respect to which the red spectrum becomes topologically non-trivial. Throughout the manuscript, we set the parameter  $\alpha = \frac{3\pi}{2T}$ .

For regularized dynamics (RD) this gives the fundamental relation

$$\bar{C} \stackrel{(\text{RD})}{=} \frac{1}{2} W(\Gamma) \quad (15)$$

where regularized dynamics requires that (i) the dominant eigenvalues of the Floquet propagator have modulus one, (ii) all other eigenvalues have modulus infinitesimally close to zero, and (iii) the corresponding eigenvectors are mutually orthogonal. The factor  $\frac{1}{2}$  arises from our definition of the lattice constant: in our convention, one lattice unit corresponds to the distance between neighboring unit cells, whereas in Ref. [27] it is defined as the distance between adjacent sublattice sites. Figure 2(a) shows the topological winding number as a function of the system parameters  $\beta$  and  $\gamma$ .

## B. Winding number and transport

For our model, specifically in the dissipative sub-period, the non-Hermitian Hamiltonian reads

$$H_{\text{NH}} = (-i) \frac{\gamma}{4} \sum_j \psi_j^\dagger (\mathbb{1} + \sigma_z) \psi_j. \quad (16)$$

In the special case of perfectly helical unitary dynamics ( $\alpha = \beta = \frac{3\pi}{2T}$ ) [40] in the coherent sub-periods, the total non-unitary Floquet operator  $F(k)$  reads

$$F(k) = \begin{pmatrix} e^{ik - \frac{\gamma T}{6}} & 0 \\ 0 & e^{-ik} \end{pmatrix} = \begin{pmatrix} \xi_-(k) & 0 \\ 0 & \xi_+(k) \end{pmatrix} \quad (17)$$

and thus leads to an imaginary splitting of the eigenvalues  $\xi_{\pm}(k)$  due to damping of the right-moving mode. Furthermore, for  $\gamma \rightarrow \infty$  the demands of regularized dynamics are fulfilled and the transport is quantized with  $\bar{C} = \frac{1}{2} W(\frac{1}{2}) = \frac{1}{2}$ . However, this particular limit is only

achieved by fully damping one of the two modes which – in the context of open quantum systems – may be seen as unphysical, since quantum jumps were ignored.

In Fig. 2 we show the topological winding number and the mean transferred charge  $\bar{C}(p)$  for  $p = 1$  and  $p = 2$  of the non-Hermitian Floquet chain. To calculate the winding number, we numerically check if the two eigenvalue bands are separated by an imaginary gap  $\Gamma$  and calculate the winding number  $W(\Gamma)$  (see Eq. (12)). With the onset of dissipation  $\gamma > 0$ , a non-zero winding number emerges at  $\frac{\beta T}{3} = \frac{\pi}{2}$  as the two eigenvalue circles of the perfect-momentum locking Hamiltonian split. As  $\gamma$  increases, the non-trivial topology extends to arbitrarily small values of  $\beta$ . However, for  $\beta = 0$ , we will never reach a topologically non-trivial phase because the  $k$ -dependence of the eigenvalues vanishes

$$F(k) = \begin{pmatrix} 0 & ie^{ik} \\ ie^{-ik - \frac{\gamma T}{6}} & 0 \end{pmatrix} \Rightarrow \xi_{\pm}(k) = \pm ie^{-\frac{\gamma T}{12}} \quad (18)$$

In contrast to the system's topological properties, the mean transferred charge after a single Floquet cycle (cf. 2(b)) can point in either direction depending on the parameters, while still being non-reciprocal in each case. This behavior can be traced back to the microdynamics: the spin-down component of the initial state remains unaffected by dissipation, whereas the spin-up component is partially depleted, then rotated by  $H_1$  and transported via  $H_2$ . The resulting asymmetry induces non-reciprocal motion, but leftward transport is merely a transient one-cycle effect – after this first cycle, the part of the state transferred to the left is in a spin-up configuration and is subsequently removed by the system's non-Hermiticity (cf. 2(c)). For  $\frac{\beta T}{3} \neq \frac{\pi}{2}$ , the rightward transport also gradually diminishes, since the spin-down component is slightly rotated by the non-optimal  $\beta$ , producing a spin-up fraction that is subsequently removed by dissipation. Consequently, under the effective non-Hermitian time evolution, the initial spin-down component – and thus the

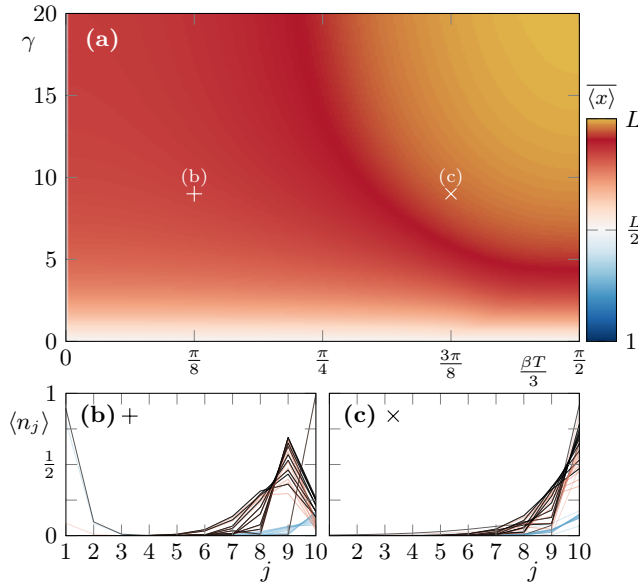


Figure 3. Eigenstate localization of the non-unitary Floquet operator  $F$  under open boundary conditions for a chain of length  $L = 10$ . (a) Mean localization  $\langle x \rangle = \frac{1}{2L} \sum_{a=1}^{2L} \langle \varphi_a | x | \varphi_a \rangle$  of the eigenstates  $|\varphi_a\rangle$  as a function of the system parameters  $\beta$  and  $\gamma$ . The parameter sets  $(\frac{\beta T}{3}, \gamma) = (\frac{\pi}{8}, 9)$  and  $(\frac{3\pi}{8}, 9)$  are highlighted, with their corresponding right eigenstates shown in panels (b) and (c). (b,c) Spatial distributions  $\langle \varphi_a | n_j | \varphi_a \rangle$  (black) together with spin-resolved components  $\langle \varphi_a | n_{js} | \varphi_a \rangle$  for  $s = \uparrow$  (red) and  $s = \downarrow$  (blue). Note the presence of a single eigenstate localized at the left edge of the chain in (b).

sustained non-reciprocal transport – can only persist for the optimal value of  $\beta$ .

In summary, for our model within the topological phase, non-reciprocal transport proceeds from the second Floquet period onwards in the direction dictated by the topological winding number. Quantization of the transported charge occurs only in the limit of the regularized dynamics. Nevertheless, the presence of a topological phase does not guarantee stable transport; this is ensured only in the regularized limit. From the perspective of the quantum master equation, however, this limit should be viewed critically, since it relies on the idealized assumption that quantum jumps can be neglected.

### C. Non-Hermitian skin effect

With open boundaries, non-reciprocal transport may lead to an accumulation of the quantum state on one of the boundaries. The accumulation of eigenstates of the Hamiltonian at the edge is called the non-Hermitian skin effect (NHSE). In order to investigate the extent to which our system exhibits NHSE and how this relates to the topological winding number, we consider the system with open boundary conditions in this section.

In particular, we calculate the normalized (right) eigenstates  $|\varphi_a\rangle$  of the non-unitary Floquet operator  $F$  and

investigate their localization  $\langle \varphi_a | x | \varphi_a \rangle$ .

In Fig. 3 we show the mean localization (see Subfigure (a)) as well as the states of two specific parameter choices for  $\beta$  and  $\gamma$  (see Subfigures (b,c)). From the mean localization one can see that as  $\gamma$  increases, an extensive number of states accumulates on the right side of the chain. In fact, for optimal  $\frac{\beta T}{3} \rightarrow \frac{\pi}{2}$  and strong dissipation  $\gamma$  every eigenstate of  $F$  localizes on the right boundary. Interestingly, there are two isolated modes with vanishing imaginary part (the OBC spectrum of  $F$  is not shown here), one of which is localized on the right boundary and the other moves to the left boundary as  $\beta \rightarrow 0$  as demonstrated by the Fig. 3(b). The above numerical results show that the existence of non-Hermitian skin effect with open boundary conditions is closely related to the nonzero winding number of the spectrum with periodic boundary conditions. This correspondence resembles the topological origin of non-Hermitian skin effect in static systems [62, 63].

## IV. OPEN QUANTUM SYSTEM

In the following, we will investigate the open quantum system including quantum jump terms in Eq. (1). To this end, we introduce a Fourier transform that block-diagonalizes the vectorized Lindblad-Floquet operator allowing to generalize the idea of a winding number to translation invariant Liouvillians. Afterwards, we investigate the dynamics of the open quantum system for closed boundaries and the steady state for open boundaries.

### A. Embedding of non-Hermitian topology to Liouvillians

Even though the jump operators  $L_\kappa$  in the Lindblad master equation (1) act on the density matrix  $\rho$  from both sides, it is a linear differential equation in the density matrix  $\rho$ . Thus, we may transform the Lindblad master equation into the usual form  $\frac{d}{dt} |\rho(t)\rangle\rangle = \mathcal{L} |\rho(t)\rangle\rangle$  of a linear equation by vectorizing the density matrix  $\rho \rightarrow |\rho\rangle\rangle$  [64]. The Lindblad superoperator  $\mathcal{L}$  is then represented as a square matrix  $\mathcal{L}$  acting on the vectorized density matrix  $|\rho\rangle\rangle$  from the left only.

This differential equation can be solved by matrix-exponentiation if the Lindblad superoperator does not explicitly depend on time  $t$ . Thus, for each Liouvillian  $\mathcal{L}_i$  we have

$$|\rho(t + \Delta t)\rangle\rangle = \exp(\mathcal{L}_i \Delta t) |\rho(t)\rangle\rangle. \quad (19)$$

In particular, the Floquet-Liouvillian propagator  $\mathcal{F}$ , which describes the stroboscopic dynamics after a full Floquet cycle, reads

$$\mathcal{F} = \exp(\mathcal{L}_3 T/3) \exp(\mathcal{L}_2 T/3) \exp(\mathcal{L}_1 T/3). \quad (20)$$

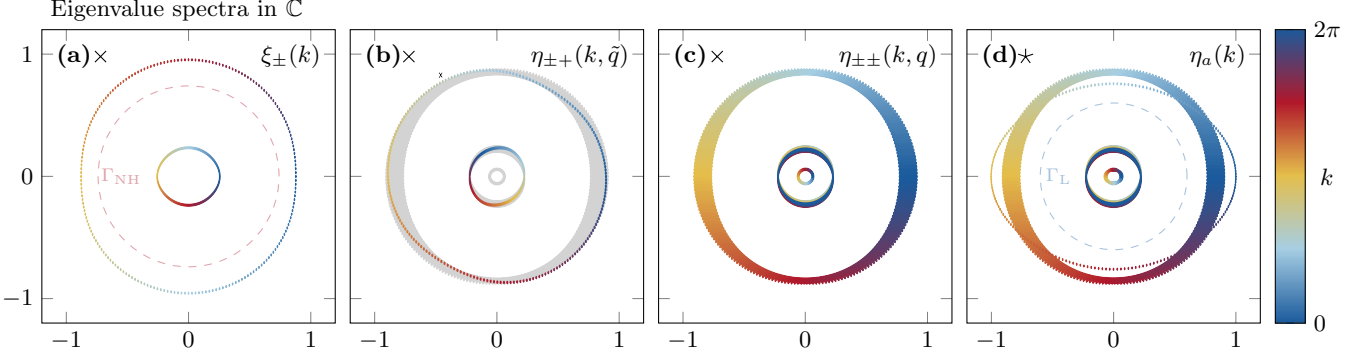


Figure 4. Spectral distributions in the punctured complex plane and their dependence on momentum  $k$ . (a)  $\xi_{\pm}(k)$  of the non-unitary Floquet operator  $F(k)$ ; the dashed red circle shows a choice of an imaginary gap  $\Gamma_{\text{NH}}$ , with respect to which the spectrum becomes topologically non-trivial. (b)  $\eta_{\pm+}(k, \tilde{q}) = \xi_{\pm}(\tilde{q} - k)\xi_{\pm}^*(\tilde{q})$  from the no-jump Floquet-Liouvillian propagator  $\mathcal{F}^{\text{NH}}(k, q) = F(q - k) \otimes F^*(q)$ , shown versus  $k$  for fixed  $\tilde{q} = 2\pi \frac{33}{L}$ . (c)  $\eta_{\pm\pm}(k, q)$  as functions of  $k$ . (d)  $\eta_a(k)$  of the full Floquet-Liouvillian propagator  $\mathcal{F}(k)$  for the open Floquet chain; the dashed blue circle shows a choice of an imaginary gap  $\Gamma_{\text{L}}$ , with respect to which the spectrum becomes topologically non-trivial. For all plots the parameters chosen are  $\alpha = \frac{3\pi}{2T}$ ,  $\beta = \frac{3}{4}\frac{3\pi}{2T}$ ,  $\gamma = 9$  and  $L = 200$  unit cells.

As a short-hand notation for the stroboscopic time-evolution of the system, we will henceforth use

$$|\rho(t + T)\rangle\rangle = \mathcal{F}|\rho(t)\rangle\rangle \Leftrightarrow \rho(t + T) = \mathcal{F}[\rho(t)]. \quad (21)$$

Further, we use the notation  $\rho(t + pT) = \mathcal{F}^p[\rho(t)]$  for  $p$  Floquet steps.

A usual vectorization scheme just orders each column of the density matrix one below the other and thus does not take into account the crucial translation invariance of the system (cf. Eq. 7). Due to the translation invariance of the Liouvillians (and thus of the Floquet operator), there exists a momentum variable  $k$  which block-diagonalizes the Floquet operator. To this end, we apply a Fourier transform along the diagonal of the density matrix

$$\rho_{\Delta}^{ss'}(k) = \frac{1}{\sqrt{L}} \sum_j e^{-ikj} |j, s\rangle\langle j + \Delta, s'|. \quad (22)$$

The vectorized state is then written as  $\rho_{\Delta}^{ss'}(k) \rightarrow |k; \Delta, s, s'\rangle\rangle$ .

In this particular lattice-momentum space, the Liouvillians are diagonal with respect to  $k$  and can be written as

$$\mathcal{L}_1(k) = (-i\beta) [\mathbb{1} \otimes (\sigma_x \oplus (-\sigma_x))] \quad (23)$$

$$\begin{aligned} \mathcal{L}_2(k) = (i\alpha) & [T_{-1} \otimes ((e^{ik}\sigma_-) \oplus (-\sigma_+))] \\ & + T_1 \otimes ((e^{-ik}\sigma_+) \oplus (-\sigma_-)) \end{aligned} \quad (24)$$

$$\mathcal{L}_-(k) = \gamma \left( \mathcal{L}_-^{\text{NH}} + \mathcal{L}_-^{\text{jumps}} \right) \quad (25)$$

$$\mathcal{L}_-^{\text{jumps}} = \delta_{\Delta=0} \otimes \sigma_- \otimes \sigma_- \quad (26)$$

$$\mathcal{L}_-^{\text{NH}} = -\frac{1}{2} [\mathbb{1}_L \otimes (\sigma_+ \sigma_- \oplus \sigma_+ \sigma_-)] \quad (27)$$

where  $\otimes$  denotes the Kronecker product,  $A \oplus B = A \otimes \mathbb{1} + \mathbb{1} \otimes B$  the Kronecker sum and  $T_a$  is the translation

operator. Obviously, the Lindblad-Floquet superoperator is diagonal with respect to  $k$  as well

$$\mathcal{F} = \sum_{\nu_1, \nu_2} \mathcal{F}_{\nu_1 \nu_2}(k) |k; \nu_1\rangle\langle k; \nu_2| \quad (28)$$

with the multi-indices  $\nu_i = (\Delta_i, s_i, s'_i)$ . The matrix  $\mathcal{F}(k)$  is a  $4L \times 4L$  matrix whose eigenvalues we denote by  $\eta_a(k)$  with  $a \in \{1, 2, \dots, 4L\}$ . For a more detailed derivation of this equations, see Appendix A.

In order to get insights to the topological structure of the full Lindblad-Floquet operator, we first note that the non-Hermitian approximation (ignoring  $\gamma \delta_{\Delta=0} \otimes \sigma_- \otimes \sigma_-$  in  $\mathcal{L}_-(k)$ ) is translation-invariant with respect to  $\Delta$  as well. Applying another Fourier transform (momentum variable  $q$ ) and using the properties of the Kronecker sum, we get

$$\mathcal{F}^{\text{NH}}(k, q) = F(q - k) \otimes F^*(q) \quad (29)$$

where  $F$  is the non-Hermitian Floquet operator in momentum space (see Eq. (11)). This specific structure allows to read the eigenvalues of  $\mathcal{F}^{\text{NH}}(k, q)$  as  $\eta_{\pm\pm}(k, q) = \xi_{\pm}(q - k)\xi_{\pm}^*(q)$ . If we consider  $\eta_{\pm\pm}(k, \tilde{q})$  (with  $q = \tilde{q}$  fixed) as  $\xi_{\pm}(\tilde{q} - k)$  being linearly scaled with the complex number  $\xi_{\pm}^*(\tilde{q}) \neq 0$ , we can calculate the non-Hermitian winding number  $W(\Gamma)$  by calculating the winding number of  $\eta_{\pm\pm}(k, \tilde{q})$ . Note that the existence of an imaginary gap  $\Gamma$  separating  $\xi_{\pm}$  forces the existence of two imaginary gaps  $\Gamma_1$  and  $\Gamma_2$  separating the eigenvalue sets  $\{\eta_{++}\}, \{\eta_{+-}, \eta_{-+}\}$  and  $\{\eta_{--}\}$ . Also, the specific choice of  $\tilde{q}$  is irrelevant for the topological properties.

Fig. 4 illustrates the transformation for a topologically non-trivial parameter set – starting from the NH Floquet operator, through the Liouvillian without quantum jumps to the full Lindbladian. One observes that one of the two eigenvalue branches  $\xi_{\pm}(k)$  of the NH Floquet operator  $F$  (specifically  $\xi_+(k)$  in Fig. 4(a)) gives rise to two distinct

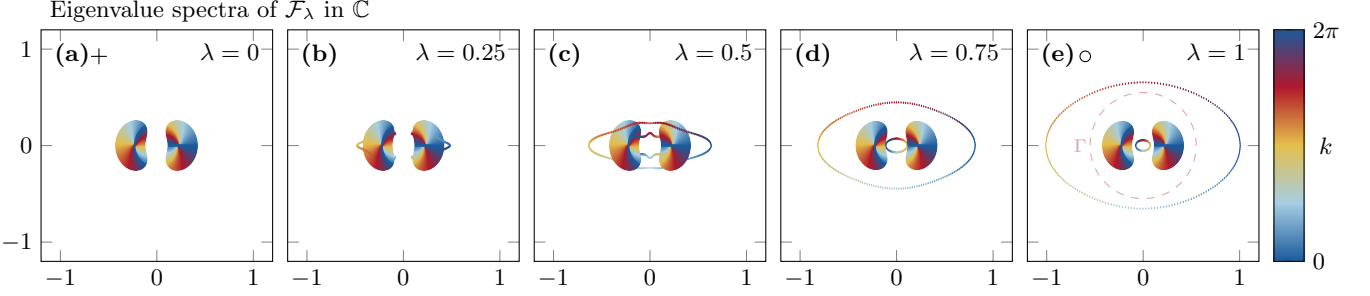


Figure 5. Spectral distributions of the interpolation between the no-jump Floquet-Liouvillian propagator  $\mathcal{F}^{\text{NH}}(k)$  and the fully open Floquet-Liouvillian propagator  $\mathcal{F}(k)$ . The parameter  $\lambda$  is defined by  $\mathcal{L}_\lambda(t)[\rho] = -i(H_{\text{NH}}(t)\rho - \rho H_{\text{NH}}^\dagger(t)) + \lambda \sum_\kappa \gamma_\kappa(t) L_\kappa \rho L_\kappa^\dagger$ . For all plots the parameters chosen are  $\alpha = \frac{3\pi}{2T}$ ,  $\beta = \frac{1}{4} \frac{3\pi}{2T}$ ,  $\gamma = 9$  and  $L = 200$  unit cells. (d) A non-trivial topology has emerged from the inclusion of quantum jumps; the dashed red circle shows a choice of an imaginary gap  $\Gamma$ , with respect to which the spectrum becomes topologically non-trivial.

eigenvalue branches  $\eta_{\pm\pm}(k, \tilde{q})$  for each value of  $\tilde{q}$ , which remain separated from each other (see Fig. 4(b)). The complete set of eigenvalues  $\eta_{\pm\pm}(k, q)$  thus forms three distinct regions: the innermost corresponding to  $\eta_{--}(k, q)$ , the middle one to  $\eta_{+-}(k, q)$  and  $\eta_{-+}(k, q)$ , and the outermost to  $\eta_{++}(k, q)$  (see Fig. 4(c)). For  $\eta_{++}(k, q)$ , each individual curve  $\eta_{++}(k, \tilde{q})$  possesses a topological winding number that is opposite in sign to that of  $\xi_+(k)$ . In total,  $\eta_{++}(k, q)$  consists of  $L$  eigenvalue curves, each sharing the same winding number. Accordingly, we associate the broadened eigenvalue band  $\eta_{++}$  with the topological winding number of  $\xi_+(k)$ . Analogously, the same correspondence holds for  $\eta_{--}(k, \tilde{q})$ . In contrast, for the middle region, the windings of the eigenvalue curves  $\eta_{+-}(k, \tilde{q})$  and  $\eta_{-+}(k, \tilde{q})$  are opposite and thus cancel each other, leading to a total winding number of  $W = 0$ . The large number of eigenvalue curves originates from the doubled Hilbert space, which also accounts for the classical coherences of the states.

## B. Topology of open quantum Floquet chains

Including the quantum jumps, this simple relation in Eq. (29) gets destroyed because the translation invariance with respect to  $\Delta$  is lost. Indeed, for our simple model, we find that for each  $k$ , the quantum jumps pose a low-rank perturbation to the Lindblad-Floquet propagator since it only acts on  $\Delta = 0$  (see Appendix A). The spectrum of low rank perturbations, that is, of matrices of the form  $A + \delta A$  where  $\delta A$  has low rank, is an active field of mathematical research [65–69]. In several studied cases, the majority of eigenvalues are only weakly affected, whereas a few eigenvalues are shifted far away from the bulk spectrum. For low-rank perturbations on a non-normal matrix, such a simple picture generally does not hold, as the entire spectrum may be shifted. Nevertheless, even though  $\mathcal{F}(k)$  is generally not a normal matrix, our numerical studies show that at most two outliers  $\eta_{\pm\pm}(k)$  appear for each  $k$  (cf. Figs. 4 and 5). This behavior can be seen in

Fig. 5 where the appearance of such a dominant outlier is demonstrated by continuously switching on jump terms within the Lindblad master equation, i.e. we define

$$\mathcal{L}_\lambda[\rho] = -i(H_{\text{NH}}\rho - \rho H_{\text{NH}}^\dagger) + \lambda \sum_\kappa \gamma_\kappa L_\kappa \rho L_\kappa^\dagger \quad (30)$$

where  $\mathcal{L}_\lambda$ ,  $H_{\text{NH}}$  and  $\gamma_\kappa$  formally depend on the time  $t$ , and the Floquet propagator  $\mathcal{F}_\lambda$  similar to before (see Eq. (20)). In Fig. 5 one can see that as  $\lambda$  goes from 0 to 1, two outlier curves  $\eta_{\pm\pm}(k)$  appear while the bulk spectrum remains essentially unchanged. One of those outliers  $\eta_{\pm\pm}(k)$  eventually dominates the spectrum and thus the dynamics.

However, there are also parameter combinations where the bulk spectrum and outliers are comparable in magnitude as it can be seen in Fig. 4. In this case, we do not a priori know which states carry the transport, since the eigenstates of the Liouvillian are not necessarily physical density matrices and can also represent coherences between states, which do not correspond to direct transport processes. We define the winding number of an individual band  $\eta_a(k)$  by

$$\mathcal{W}(\eta_a) = \frac{(-i)}{2\pi} \int_{-\pi}^{\pi} \eta_a(k)^{-1} \partial_k \eta_a(k) dk. \quad (31)$$

Further, we define the system winding number  $\mathcal{W}_S$  by two distinct cases: (i) if the outlier is separated from the bulk states by an imaginary gap, the topological winding number is the winding number of the outlier (cf. Fig. 5(e)), (ii) if the outlier and the bulk states are comparable in magnitude and all states have the same winding number, the topological winding number is the shared winding number of all states (cf. Fig. 4(d)). Mathematically, we define the set  $S_\Gamma(k) = \{\eta_a(k) : |\eta_a(k)| > \Gamma\}$  and calculate the winding number for each state within  $S_\Gamma(k)$  yielding another set  $\mathcal{W}_\Gamma = \{\mathcal{W}(\eta_a) : \eta_a \in S_\Gamma\}$ . If  $\mathcal{W}_\Gamma$  contains only a single winding number  $\mathcal{W}_\Gamma = \{\mathcal{W}_o\}$ , this must be the winding number of the outlier and we take it as the winding number of the whole system  $\mathcal{W}_S = \mathcal{W}_o$ . If  $\mathcal{W}_\Gamma$  contains exactly  $L$  winding numbers ( $|\mathcal{W}_\Gamma| = L$  where

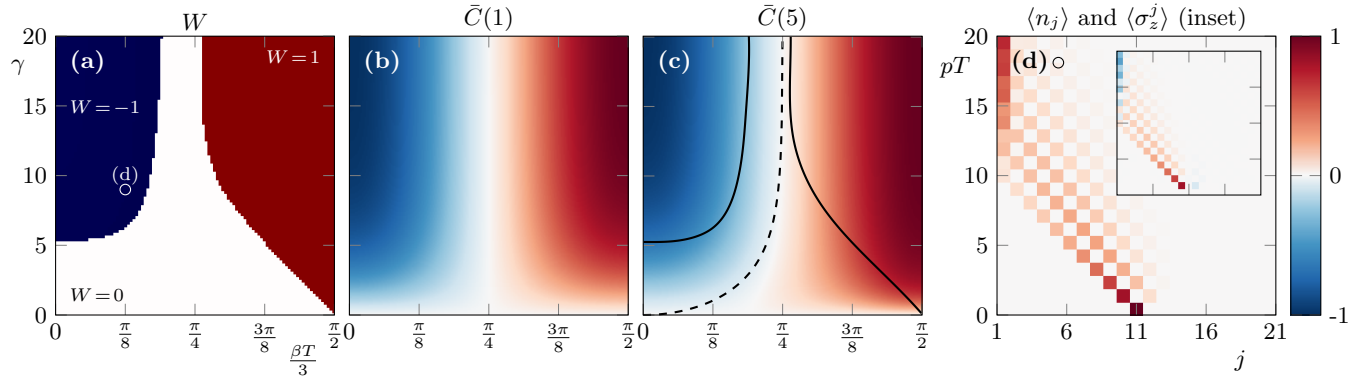


Figure 6. (a) Topological winding number as a function of the parameters  $\beta$  and  $\gamma$ . The parameter set  $(\frac{\beta T}{3}, \gamma) = (\frac{\pi}{8}, 9)$  is highlighted and used for the time evolution in Figure (d). (b,c) Mean transferred charge  $\bar{C}(p)$  after  $p = 1$  (b) and  $p = 5$  (c) Floquet cycles, plotted versus  $\beta$  and  $\gamma$ . The solid lines in (c) indicate the contour lines of the topological phases shown in (a), while the dashed line corresponds to  $\gamma = -\frac{3}{T} \log \cos(\frac{2\beta T}{3})$  which has been found to phenomenologically capture the long-time limit. (d) Stroboscopic time evolution of an unpolarized fermion initially placed at the center of the open chain. Shown is the site-resolved particle number  $\langle n_j(pT) \rangle$  as a function of position  $j$  and stroboscopic time  $pT$ . The inset displays the corresponding spin polarization  $\langle \sigma_z^j(pT) \rangle$ .

$L$  is the number of unit cells) and all winding numbers are equal ( $\exists \mathcal{W}_o \in \mathcal{W}_\Gamma, \forall \mathcal{W}(\eta) \in \mathcal{W}_\Gamma : \mathcal{W}_o = \mathcal{W}(\eta)$ ), then  $\mathcal{W}_S = \mathcal{W}_o$ . Otherwise, we set  $\mathcal{W}_S = 0$ . Note that this definition is equal to defining the winding number as the winding number of the outlier as long as the bulk states are not comparable in magnitude and winding in the opposite direction.

### C. Winding number and transport

Similar to the non-Hermitian case, we define the transferred charge by  $\bar{C}_n(p) = \frac{1}{p} \langle x - n \rangle_{\rho_n(pT)}$ . In the Fourier transformed space, this can be written as (see Appendix B for the derivation)

$$\bar{C} = \frac{(-i)}{2} \sum_{s,s'} \frac{\partial}{\partial k} \mathcal{F}_{(0ss), (0s's')}(k) \Big|_{k=0} \quad (32)$$

One can see that the specific structure of  $\bar{C}$  which allowed the existence of the fundamental relation ( $\bar{C} = \frac{W}{2}$ ) arises from the Kronecker product structure of the Floquet operator in the non-Hermitian case which is destroyed in the fully open case.

Figure 6 shows the winding number, the transferred charge and the time-evolution of a single unpolarized fermion placed in the middle of the dissipative quantum chain. We observe the appearance of a new topological phase around  $\beta = 0$  and  $\gamma \approx 5.2$ , expanding rapidly toward  $\beta \rightarrow 0.5$  with increasing  $\gamma$  (see Fig. 6(a)). Note that this topological phase follows from dominant behavior of an outlier while the one on the right side comes from the collective winding of the outlier and the bulk states. Thus, the left-hand-side topological phase cannot exist without the quantum jumps and the right-hand-side topological phase can be seen as not being destroyed by quantum

jumps but a remainder of the non-Hermitian topological phase. We thus claim to have found a *quantum jump induced topology* (cf. Fig. 5). As one can see, the topological phases are characterized by winding numbers with opposite sign which is also supported by both, the skin effect and the transport properties as one can see below.

Furthermore, we observe that the mean transport after  $p = 1$  and  $p = 5$  Floquet periods (see Fig. 6(b,c)) approximately follows the topological winding number, i.e. within the topological phase, the direction of transport agrees with the winding number, although the transport is not quantized. However, for  $p = 1$  the transport is symmetric with respect to  $\frac{\beta T}{3} = \frac{\pi}{4}$ , whereas for  $p > 1$  this symmetry is broken, consistent with the asymmetry of the underlying topological phases. In particular, the phase transition, at which the transport changes direction, is compatible with  $\gamma = -\frac{3}{T} \log \cos(\frac{2\beta T}{3})$  in the long-time limit (see dashed line in Fig. 6(c)). This expression, up to a factor of 2, coincides with the phase boundary between positive and negative steady-state spin polarizations for the single-site model studied in Appendix C.

In Figure 6(d) we show the stroboscopic time-evolution of an unpolarized fermion placed in the middle of the quantum chain with open boundary conditions. Here, the main plot shows the expectation value of the particle number  $\langle n_j(pT) \rangle$  and the inset shows the expectation value of the spin polarization  $\langle \sigma_z^j(pT) \rangle$ . One can see that, for these parameters, the fermion moves continuously to the left, becoming partially delocalized during its motion, but eventually reaches the boundary, where it becomes trapped in the spin-down state.

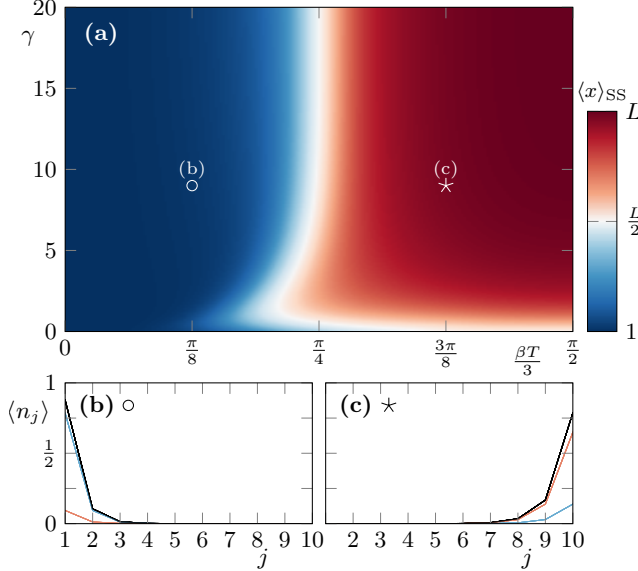


Figure 7. Steady state localization of Floquet-Liouvillian propagator  $\mathcal{F}$ . (a) Localization  $\langle x \rangle_{ss} = \text{Tr}[x \rho_{ss}]$  of the steady state  $\rho_{ss}$  (only eigenstate with unit trace) as a function of the system parameters  $\beta$  and  $\gamma$ . The parameter sets  $(\frac{\beta T}{3}, \gamma) = (\frac{\pi}{8}, 9)$  and  $(\frac{3\pi}{8}, 9)$  are highlighted, with their corresponding eigenstates shown in panels (b) and (c). (b,c) Spatial distributions  $\text{Tr}[n_j \rho_{ss}]$  (black) together with spin-resolved components  $\text{Tr}[n_{j\sigma} \rho_{ss}]$  for  $\sigma = \uparrow$  (red) and  $\sigma = \downarrow$  (blue).

#### D. Steady state localization

Here, we investigate the localization of the steady state of the Floquet operator  $\mathcal{F}$  with open boundaries. Figure 7(a) shows the localization  $\text{Tr}[x \rho_{ss}]$  and Figs. 7(b-c) show two specific parameter sets  $\beta, \gamma$ . We find that the localization looks qualitatively very similar to the transferred charge after many Floquet steps. However, the nose that can be seen at  $\gamma \approx 1, \frac{\beta T}{3} \approx \frac{\pi}{6}$  can be traced back to a finite size effect. In the thermodynamic limit  $L \rightarrow \infty$  the white line, where the steady state is not localized at one side, extends to  $\beta = 0, \gamma = 0$  without bending back.

#### V. TOWARD EXPERIMENTAL REALIZATION

In this section, we take a look at an experimentally more feasible version of the model. To this end, we include dephasing terms described by local Lindblad operators  $L_j^z = \psi_j^\dagger \sigma_z \psi_j$  and with dissipation rate  $\gamma_z(t)$ . Furthermore, we consider dissipation at all times  $t$ , which we describe using the following protocol

$$\gamma^{(-/z)}(t) = \begin{cases} \gamma^{(-/z)} & \text{if } t \in [0, \frac{T}{3}), \\ r\gamma^{(-/z)} & \text{if } t \in [\frac{T}{3}, T]. \end{cases} \quad (33)$$

Here we include a prefactor  $r$  which can be experimentally achieved by either engineering the actual dissipation

rates or, practically simpler, staying longer withing in the waiting phase.

In Figure 8 we show the results for the winding number, the transferred charge  $\bar{C}$  and the steady state localization. One can see that the winding number explains the transferred charge and the steady state localization roughly.

#### VI. CONCLUDING REMARKS

In this work, we have introduced a first generalization of Floquet non-Hermitian topology to open quantum systems. Our framework builds on the spectral structure of the Liouvillian superoperator and its relation to transport in dissipative Floquet systems. Specifically, we defined a topological winding number – extending the construction of Ref. [27] – which arises from the product structure of the no-jump Liouvillian and quantifies the  $k$ -dependent winding of eigenvalues around the origin of the complex plane. The inclusion of quantum jumps produces a noticeable shift of a small number of eigenvalues. We identify the system's topological winding number with that of an

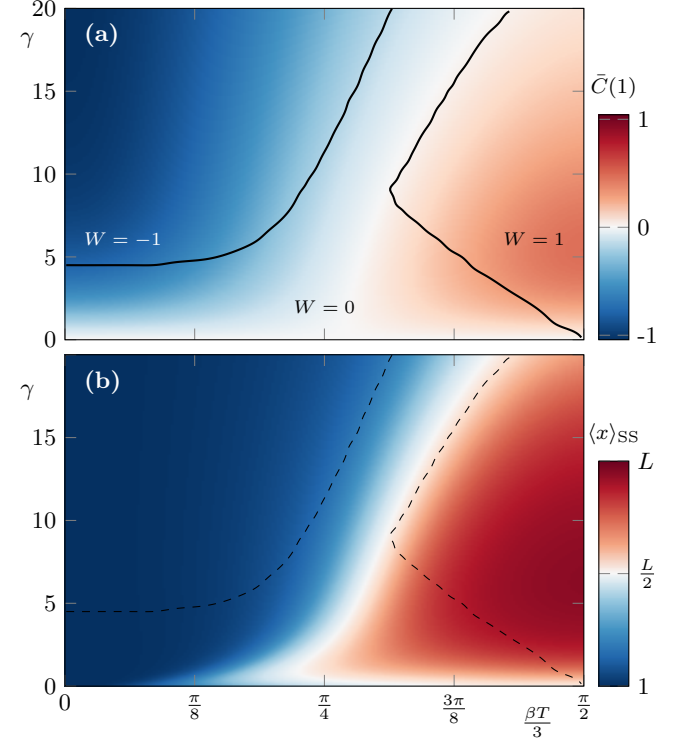


Figure 8. Mean transferred charge, steady state localization and topological winding number for a realistic model with spontaneous decay and dephasing. Parameters are  $\gamma_- = \frac{\gamma_z}{10} = \gamma$  and  $r = \frac{1}{10}$ . Shown as heatmaps over  $\beta$  and  $\gamma$ : (a) Transferred charge  $\bar{C}(1)$ , (b) Localization  $\langle x \rangle_{ss} = \text{Tr}[x \rho_{ss}]$  of the steady state  $\rho_{ss}$ . The topological phase boundaries of the winding number  $W$  are indicated by solid lines in (a) and dashed lines in (b).

outlier mode, defined either (a) as the dominant spectral contribution or (b) as the mode that winds in the same direction as the bulk without dominating it. This leads to a richer topological phase diagram than that of the effective non-Hermitian approximation.

While this construction provides a consistent description of topology in dissipative dynamics, its formulation can be refined further. A more systematic separation between populations and coherences could be achieved by introducing a weighting function over the eigenmodes, quantifying the extent to which each mode contributes to transport-relevant populations versus non-transporting coherences. Such an approach could help establish a more natural and physically grounded definition of topological winding in open quantum systems.

## VII. ACKNOWLEDGMENTS

We would like to thank Carl Lehmann for discussions. We acknowledge financial support from the German Research Foundation (DFG) through the Collaborative Research Centre SFB 1143 (Project-ID 247310070), the Cluster of Excellence ct.qmat (Project-ID 390858490), and the DFG Project No. 459864239. Our numerical calculations were performed on resources at the TU Dresden Center for Information Services and High Performance Computing (ZIH).

## Appendix A: Vectorization of the translation-invariant, single-particle space

In this section, we give a more detailed version of the vectorization scheme we used. For the quantum system, we chose  $|m, s\rangle = |m\rangle \otimes |s\rangle$  as the basis states, where  $m$  denotes the site and  $s$  the spin configuration. The density matrix can then be written as

$$\rho = \sum_{m, m'} \sum_{s, s'} \rho_{(ms), (m's')} |m, s\rangle \langle m', s'|. \quad (\text{A1})$$

We are vectorizing the density matrix by defining the new basis states  $|m, s\rangle \otimes (\langle m', s' |)^T$  and then (using the separation of spatial and spin components) changing the order of the parameters to

$$|m, m', s, s'\rangle = |m\rangle \otimes \langle m'|^T \otimes |s\rangle \otimes \langle s'|^T \quad (\text{A2})$$

and mapping the density matrix to

$$\rho \rightarrow |\rho\rangle\rangle = \sum_{m, m'} \sum_{s, s'} \rho_{(ms), (m's')} |m, m', s, s'\rangle\rangle. \quad (\text{A3})$$

The Lindblad master equation (Eq. (1)) is acting onto the density matrix from the left and the right. Using the non-Hermitian Hamiltonian (see Eq. 9), it can be written as

$$\dot{\rho} = -i(H_{\text{NH}}\rho - \rho H_{\text{NH}}^\dagger) + \sum_{\kappa} \gamma_{\kappa} L_{\kappa} \rho L_{\kappa}^\dagger \quad (\text{A4})$$

where the NH Hamiltonian is acting *either* from the left or the right and it can be written generically as

$$H_{\text{NH}} = \sum_{m, m'} \sum_{s, s'} h_{(ms), (m's')} |m, s\rangle \langle m', s'|. \quad (\text{A5})$$

Assuming translation invariance,

$$[H_{\text{NH}}, T_1] = 0, \quad T_1 = \sum_m |m+1\rangle \langle m| \otimes \mathbb{1}_2, \quad (\text{A6})$$

it follows that the matrix elements depend only on the distance  $\delta = m - m'$ :

$$h_{(ms), (m's')} = h_{ss'}^{m-m'} \equiv h_{s,s'}^{\delta}. \quad (\text{A7})$$

Therefore, the Hamiltonian can be written as a sum of tensor products of spatial and spin operators:

$$H_{\text{NH}} = \sum_{\delta} R_{\delta} \otimes S_{\delta}, \quad (\text{A8})$$

where the spatial component is

$$R_{\delta} = \sum_m |m+\delta\rangle \langle m|, \quad (\text{A9})$$

and the spin component is

$$S_{\delta} = \sum_{s, s'} h_{ss'}^{\delta} |s\rangle \langle s'|. \quad (\text{A10})$$

Optionally, for spin- $\frac{1}{2}$ , one can further expand  $S_{\delta}$  in the Pauli basis:

$$S_{\delta} = c_{\delta} \mathbb{1} + \vec{v}_{\delta} \cdot \vec{\sigma}. \quad (\text{A11})$$

The vectorization of the von-Neumann-like part of the Lindblad master equation then reads

$$H_{\text{NH}} |m, s\rangle \langle m', s'| - |m, s\rangle \langle m', s'| H_{\text{NH}}^\dagger \quad (\text{A12})$$

$$\rightarrow (H_{\text{NH}} \otimes \mathbb{1} - \mathbb{1} \otimes H_{\text{NH}}^*) |m, s\rangle \otimes \langle m', s'|^T \quad (\text{A13})$$

$$\begin{aligned} &\rightarrow \sum_{\delta} (T_{\delta} \otimes \mathbb{1}_L \otimes S_{\delta} \otimes \mathbb{1}_2 \\ &\quad - \mathbb{1}_L \otimes T_{\delta} \otimes \mathbb{1}_2 \otimes S_{\delta}^*) |m, m', s, s'\rangle \end{aligned} \quad (\text{A14})$$

Additionally, we also have the so-called quantum jump terms  $L_{\kappa} \rho L_{\kappa}^\dagger$ , the ( $\gamma_{\kappa}$ -weighted) sum of which is translation-invariant by translation with a single site ( $T_1 \mathcal{J}[\rho] T_1^\dagger = \mathcal{J}[T_1 \rho T_1^\dagger]$  with  $\mathcal{J}[\rho] = \sum_{\kappa} \gamma_{\kappa} L_{\kappa} \rho L_{\kappa}^\dagger$ ) as well. Here, we only focus on dissipative processes that locally flip the spin at a single site, e.g.

$$L_m^{\kappa} = |m\rangle \langle m| \otimes S_{\kappa} \quad (\text{A15})$$

The total dissipative contribution to the dynamics is then obtained by applying this process at every site

$$\mathcal{J}[\rho] = \sum_{\kappa} \sum_m L_m^{\kappa} \rho (L_m^{\kappa})^\dagger. \quad (\text{A16})$$

which ensures translation invariance. The quantum jump terms can then be written as

$$\mathcal{J}[|m, s\rangle\langle m', s'|] \rightarrow \sum_{\kappa} P \otimes S_{\kappa} \otimes S_{\kappa}^* |m, m', s, s'\rangle \quad (\text{A17})$$

with  $P = \sum_m |m\rangle\langle m| \otimes |m\rangle\langle m|$  is a  $L^2 \times L^2$  matrix. In the case of spontaneous decay, we represent  $S_- \rightarrow \sigma_-$ , and for dephasing  $S_z \rightarrow \sigma_z$ . Note that the spin operators  $S_{\delta}$  appearing in the NH Hamiltonian and  $S_{\kappa}$  in the jump operators are neither identical nor independent, but must be chosen consistently such that the Lindblad master equation is satisfied.

At this point we can write the vectorized Liouvillians in real space representation as follows:

$$\mathcal{L}_1 = (-i\beta) [\mathbb{1}_L \otimes \mathbb{1}_L \otimes (\sigma_x \otimes \sigma_0 - \sigma_0 \otimes \sigma_x)] \quad (\text{A18})$$

$$\mathcal{L}_2 = (i\alpha) [T_{-1} \otimes \mathbb{1}_L \otimes \sigma_+ \otimes \sigma_0 + T_1 \otimes \mathbb{1}_L \otimes \sigma_- \otimes \sigma_0 - \mathbb{1} \otimes T_1 \otimes \sigma_0 \otimes \sigma_- - \mathbb{1} \otimes T_{-1} \otimes \sigma_0 \otimes \sigma_+] \quad (\text{A19})$$

$$\mathcal{L}^{\text{nj}} = -\frac{\gamma}{2} [\mathbb{1}_L \otimes \mathbb{1}_L \otimes (\sigma_+ \sigma_- \otimes \sigma_0 + \sigma_0 \otimes \sigma_+ \sigma_-)] \quad (\text{A20})$$

$$\mathcal{L}^j = \gamma [P \otimes \sigma_- \otimes \sigma_-] \quad (\text{A21})$$

Now we perform another basis transformation  $|m, m', s, s'\rangle \rightarrow |m; \Delta, s, s'\rangle$  with  $\Delta = m' - m$ . This transformation allows us to write  $P = \mathbb{1}_L \otimes \delta_{\Delta=0}$ . The Liouvillians can then be written as

$$\mathcal{L}_1 = (-i\beta) [\mathbb{1}_L \otimes \mathbb{1}_L \otimes (\sigma_x \otimes \sigma_0 - \sigma_0 \otimes \sigma_x)] \quad (\text{A22})$$

$$\mathcal{L}_2 = (i\alpha) [T_{-1} \otimes T_1 \otimes \sigma_+ \otimes \sigma_0 + T_1 \otimes T_{-1} \otimes \sigma_- \otimes \sigma_0 - \mathbb{1} \otimes T_1 \otimes \sigma_0 \otimes \sigma_- - \mathbb{1} \otimes T_{-1} \otimes \sigma_0 \otimes \sigma_+] \quad (\text{A23})$$

$$\mathcal{L}^{\text{nj}} = -\frac{\gamma}{2} [\mathbb{1}_L \otimes \mathbb{1}_L \otimes (\sigma_+ \sigma_- \otimes \sigma_0 + \sigma_0 \otimes \sigma_+ \sigma_-)] \quad (\text{A24})$$

$$\mathcal{L}^j = \gamma [\mathbb{1}_L \otimes \delta_{\Delta=0} \otimes \sigma_- \otimes \sigma_-] \quad (\text{A25})$$

We thus can perform a Fourier transform with respect to  $m$ :

$$|k; \Delta, s, s'\rangle = \frac{1}{\sqrt{L}} \sum_m e^{-ikm} |m; \Delta, s, s'\rangle \quad (\text{A26})$$

which block-diagonalizes the Liouvillians, resulting in

$$\mathcal{L}_1(k) = (-i\beta) [\mathbb{1}_L \otimes (\sigma_x \otimes \sigma_0 - \sigma_0 \otimes \sigma_x)] \quad (\text{A27})$$

$$\mathcal{L}_2(k) = (i\alpha) [e^{-ik} T_1 \otimes \sigma_+ \otimes \sigma_0 + e^{ik} T_{-1} \otimes \sigma_- \otimes \sigma_0 - T_1 \otimes \sigma_0 \otimes \sigma_- - T_{-1} \otimes \sigma_0 \otimes \sigma_+] \quad (\text{A28})$$

$$\mathcal{L}^{\text{nj}}(k) = -\frac{\gamma}{2} [\mathbb{1}_L \otimes (\sigma_+ \sigma_- \otimes \sigma_0 + \sigma_0 \otimes \sigma_+ \sigma_-)] \quad (\text{A29})$$

$$\mathcal{L}^j(k) = \gamma [\delta_{\Delta=0} \otimes \sigma_- \otimes \sigma_-] \quad (\text{A30})$$

This form of the Liouvillians is used to calculate the winding numbers for the open quantum system.

In the non-Hermitian approximation, where quantum jumps are neglected, we can further apply a similar

Fourier-transform to the  $\Delta$  index.

$$\mathcal{L}_1(q, k) = (-i\beta) [\sigma_x \oplus (-\sigma_x)] \quad (\text{A31})$$

$$\mathcal{L}_2(q, k) = (i\alpha) [(e^{-i(k-q)} \sigma_+ + e^{i(k-q)} \sigma_-) \oplus (-e^{iq} \sigma_- - e^{-iq} \sigma_+)] \quad (\text{A32})$$

$$\mathcal{L}^{\text{nj}}(q, k) = -\frac{\gamma}{2} [\sigma_+ \sigma_- \oplus \sigma_+ \sigma_-] \quad (\text{A33})$$

where we also introduced the Kronecker sum  $A \oplus B = A \otimes \mathbb{1} \otimes B$ . Using the Bloch Hamiltonians  $H_1(k) = \beta \sigma_x$  and  $H_2(k) = -\alpha [\cos(k) \sigma_x - \sin(k) \sigma_y]$ ,  $H_{\text{NH}}(k) = -\frac{i\gamma}{2} \sigma_+ \sigma_-$ , we can write the vectorized Lindbladians in the form

$$\mathcal{L}_j(q, k) = (-iH_j(q - k)) \oplus (-iH_j(q))^* \quad (\text{A34})$$

This simple form is very helpful for calculating the Lindbladian Floquet propagator

$$\mathcal{F}(q, k) = \prod_j \exp(\mathcal{L}_j(q, k) \frac{T}{3}) \quad (\text{A35})$$

$$= F(q - k) \otimes F(q)^* \quad (\text{A36})$$

where we used the matrix properties  $\exp(A \oplus B) = \exp(A) \otimes \exp(B)$ ,  $\exp(A^*) = \exp(A)^*$  and  $A^* B^* = (AB)^*$  and the NH Floquet operator  $F(k) = \prod_j \exp(-iH_j(k))$ . It allows us to link the topological behavior of the NH Floquet operator  $F(k)$  to the Lindbladian Floquet operator  $\mathcal{F}(q, k)$  by fixing a momentum  $q = \tilde{q}$ .

## Appendix B: Transferred charge in density matrix formalism

We define the mean transferred charge over one Floquet phase by

$$\bar{C} = \langle x - n \rangle_{\mathcal{F}[\rho_n(0)]} \quad (\text{B1})$$

with position operator  $x = \sum_{m,s} m |m, s\rangle\langle m, s|$ , Floquet propagator  $\mathcal{F}$  and initial state  $\rho_n(0) = \frac{1}{2} \sum_r |n, r\rangle\langle n, r|$ . After vectorizing the density matrix ( $|m, s\rangle\langle m', s'| \rightarrow |m, m', s, s'\rangle$ ), this becomes

$$\bar{C} = \frac{1}{2} \sum_m \sum_{s,r} (m - n) \langle\langle m, m, s, s | \mathcal{F} | n, n, r, r \rangle\rangle. \quad (\text{B2})$$

Applying a basis transformation  $|m, m', s, s'\rangle \rightarrow |m; \Delta = m' - m, s, s'\rangle$  and a Fourier transform  $|k; \Delta, s, s'\rangle = \frac{1}{\sqrt{L}} \sum_m e^{-ikm} |m; \Delta, s, s'\rangle$  (with inverse  $|m; \Delta, s, s'\rangle = \frac{1}{\sqrt{L}} \sum_m e^{ikm} |k; \Delta, s, s'\rangle$ ) diagonalizes the translation-invariant Floquet propagator with respect to  $k$  (see Appendix A for more details). We than have

$$\langle\langle m; \Delta, s, s' | k; \Delta', r, r' \rangle\rangle$$

$$= \text{Tr}[\langle \Delta, s' | \langle m, s | \frac{1}{\sqrt{L}} \sum_{m'} e^{-ikm'} |m', r\rangle \langle \Delta', r' |] \quad (\text{B3})$$

$$= \frac{1}{\sqrt{L}} e^{-ikm} \delta_{\Delta \Delta'} \delta_{sr} \delta_{s' r'} \quad (\text{B4})$$

which we can use to calculate the mean transferred charge

$$\bar{C} = \frac{1}{2} \sum_{s,r} \sum_m (m-n) \langle\langle m; 0, s, s | \left( \sum_k \sum_{\nu_1, \nu_2} \mathcal{F}_{\nu_1, \nu_2}(k) |k; \nu_1\rangle \langle k; \nu_2| \right) |n; 0, r, r\rangle \rangle \quad (\text{B5})$$

$$= \frac{1}{2L} \sum_{s,r} \sum_{m,k} (m-n) e^{-ik(m-n)} \mathcal{F}_{(0ss), (0rr)}(k) \quad (\text{B6})$$

$$= \frac{1}{2L} \sum_{s,r} \left[ i \frac{\partial}{\partial k} e^{-ik(m-n)} \right] \mathcal{F}_{(0ss), (0rr)}(k). \quad (\text{B7})$$

where we used the multi-indices  $\nu_i = (\Delta_i, s_i, r_i)$ . In the continuum limit this becomes

$$= \frac{1}{4\pi} \sum_{s,r} \int_0^{2\pi} \sum_m \left[ i \frac{\partial}{\partial k} e^{-ik(m-n)} \right] \mathcal{F}_{(0ss), (0rr)}(k) dk \quad (\text{B8})$$

$$= \frac{(-i)}{4\pi} \sum_{s,r} \int_0^{2\pi} \underbrace{\sum_m e^{-ik(m-n)} \left[ \frac{\partial}{\partial k} \mathcal{F}_{(0ss), (0rr)}(k) \right]}_{2\pi\delta(k)} dk \quad (\text{B9})$$

$$= \frac{(-i)}{2} \sum_{s,r} \frac{\partial}{\partial k} \mathcal{F}_{(0ss), (0rr)}(k) \Big|_{k=0} \quad (\text{B10})$$

Without the quantum jump terms, we apply another Fourier transform to the  $\Delta$ -indices and write

$$\mathcal{F}_{(\Delta ss'), (\Delta' rr')}(k) = \frac{1}{2\pi} \int_0^{2\pi} e^{-iq(\Delta-\Delta')} \mathcal{F}_{(ss'), (rr')}(k, q) dq \quad (\text{B11})$$

Further, we found  $\mathcal{F}(k, q) = F(q - k) \otimes F^*(q)$  (see Appendix A) which reads with indices inserted  $\mathcal{F}_{(ss'), (rr')}(k, q) = F_{sr}(q - k) F_{s'r'}^*(q)$ . Inserting this into the mean transferred charge, we find

$$\bar{C}^{\text{nj}} = \frac{(-i)}{4\pi} \int_0^{2\pi} \sum_{s,r} \frac{\partial}{\partial k} F_{sr}(q - k) F_{sr}^*(q) \Big|_{k=0} dq \quad (\text{B12})$$

$$= \frac{(-i)}{4\pi} \int_0^{2\pi} \sum_{s,r} \frac{\partial}{\partial k} F_{sr}(q - k) F_{rs}^\dagger(q) \Big|_{k=0} dq \quad (\text{B13})$$

$$= \frac{(-i)}{4\pi} \int_0^{2\pi} \text{Tr}_S \left[ \frac{\partial}{\partial k} F(q - k) F^\dagger(q) \right] \Big|_{k=0} dq \quad (\text{B14})$$

$$= \frac{(-i)}{4\pi} \int_0^{2\pi} \text{Tr}_S \left[ F^\dagger(q) \frac{\partial}{\partial q} F(q) \right] dq \quad (\text{B15})$$

where  $\text{Tr}_S A = \sum_\sigma A_{\sigma\sigma}$  sums over the spin degrees of freedom of the Fourier transform.

### Appendix C: Single-site open quantum system

In this appendix, we investigate a related Floquet open quantum system, which simply includes one spin degree of freedom. In other words, we turn off the couplings between different unit cells. The time evolution of the single-site density matrix  $\rho(t)$  is still controlled by the time-dependent Lindblad master equation in Eq. (1). With  $\sigma_{x,y,z}$  representing the Pauli operators for the spin degree of freedom, the full Liouvillian dynamics in one period  $T$  is given by

$$H_S(t) = \begin{cases} 0 & \text{if } t \in [0, \frac{T}{3}), \\ \beta\sigma_x & \text{if } t \in [\frac{T}{3}, \frac{2T}{3}), \\ 0 & \text{if } t \in [\frac{2T}{3}, T). \end{cases} \quad (\text{C1})$$

$$\gamma(t) = \begin{cases} \gamma & \text{if } t \in [0, \frac{T}{3}), \\ 0 & \text{if } t \in [\frac{T}{3}, T). \end{cases} \quad (\text{C2})$$

The jump operator is given by  $L = \sigma_-$ . Here, the third time interval without any dynamics is introduced to match the drive protocol for the one-dimensional system studied in the main text. The full dynamics in one period is generated by the Floquet-Liouvillian propagator  $\mathcal{F} = \exp(\mathcal{L}_3 T/3) \exp(\mathcal{L}_2 T/3) \exp(\mathcal{L}_1 T/3)$ . After the vectorization of the density matrix, the Floquet-Lindbladian superoperator has the following matrix form:

$$\mathcal{F} = \exp \left( -\frac{i\beta T}{3} (\sigma_x \oplus (-\sigma_x)) \right) \times \exp \left( \frac{\gamma T}{3} (\sigma^- \otimes \sigma^- - \frac{1}{2} \sigma^+ \sigma^- \oplus \sigma^+ \sigma^-) \right) \quad (\text{C3})$$

Defining  $\theta = \beta T/3$ ,  $G = \exp(\gamma T/6)$ , and  $D = G^2 - 2G \cos^2 \theta + 1$ , we find that the steady state density matrix  $\rho$ , which satisfies  $\mathcal{F}[\rho] = \rho$ , has the following expression:

$$\rho = \frac{1}{D} \begin{pmatrix} G^2 \sin^2 \theta & \frac{i}{2} G(G-1) \sin 2\theta \\ -\frac{i}{2} G(G-1) \sin 2\theta & D - G^2 \sin^2 \theta \end{pmatrix} \quad (\text{C4})$$

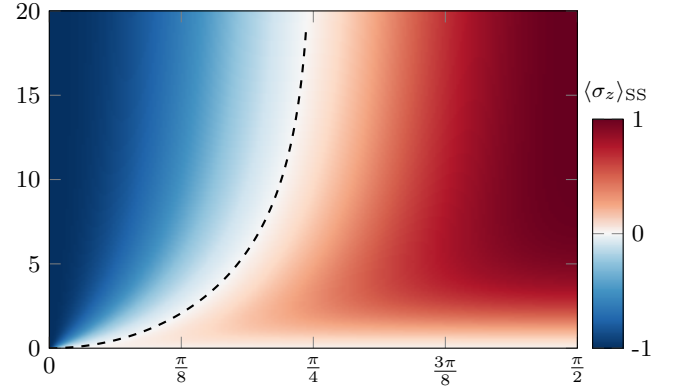


Figure 9. Expectation value of the steady-state spin polarization  $\langle \sigma_z \rangle = \text{Tr}[\sigma_z \rho_{\text{ss}}]$  of the single-site model. The dashed line displays the phase boundary where a sign change appears (cf. Eq. C6).

Based on this expression, we find that the steady-state spin polarization is given by

$$P = \text{Tr}[\rho\sigma_z] = \frac{\cos^2\theta(2G - 2G^2) - 1 + G^2}{D} \quad (\text{C5})$$

Then we can identify a phase boundary where  $P$  changes its sign. By solving  $P = 0$ , we obtain  $G \cos(2\theta) = 1$ ,

which leads to a phase boundary shown in Fig. 9:

$$\gamma = -\frac{6}{T} \log \cos\left(\frac{2\beta T}{3}\right). \quad (\text{C6})$$

After turning on the hopping between different unit cells, the different spin components prefer to move in the opposite direction, and a nonzero polarization is expected to induce chiral transport. Nevertheless, the interplay between intercell and intracell couplings will quantitatively change the phase boundary, as shown in Fig. 6(c).

---

[1] T. Kitagawa, E. Berg, M. Rudner, and E. Demler, Topological characterization of periodically driven quantum systems, *Phys. Rev. B* **82**, 235114 (2010).

[2] L. Jiang, T. Kitagawa, J. Alicea, A. R. Akhmerov, D. Pekker, G. Refael, J. I. Cirac, E. Demler, M. D. Lukin, and P. Zoller, Majorana fermions in equilibrium and in driven cold-atom quantum wires, *Phys. Rev. Lett.* **106**, 220402 (2011).

[3] T. Kitagawa, M. A. Broome, A. Fedrizzi, M. S. Rudner, E. Berg, I. Kassal, A. Aspuru-Guzik, E. Demler, and A. G. White, Observation of topologically protected bound states in photonic quantum walks, *Nat. Commun.* **3**, 10.1038/ncomms1872 (2012).

[4] M. S. Rudner, N. H. Lindner, E. Berg, and M. Levin, Anomalous edge states and the bulk-edge correspondence for periodically driven two-dimensional systems, *Phys. Rev. X* **3**, 031005 (2013).

[5] S. Vajna and B. Dóra, Topological classification of dynamical phase transitions, *Phys. Rev. B* **91**, 155127 (2015).

[6] J. C. Budich and M. Heyl, Dynamical topological order parameters far from equilibrium, *Phys. Rev. B* **93**, 085416 (2016).

[7] I. Martin, G. Refael, and B. Halperin, Topological frequency conversion in strongly driven quantum systems, *Phys. Rev. X* **7**, 041008 (2017).

[8] A. Quelle, C. Weitenberg, K. Sengstock, and C. M. Smith, Driving protocol for a floquet topological phase without static counterpart, *New J. Phys.* **19**, 113010 (2017).

[9] N. Fläschner, D. Vogel, M. Tarnowski, B. S. Rem, D.-S. Lühmann, M. Heyl, J. C. Budich, L. Mathey, K. Sengstock, and C. Weitenberg, Observation of dynamical vortices after quenches in a system with topology, *Nat. Phys.* **14**, 265 (2018).

[10] V. Junk, P. Reck, C. Gorini, and K. Richter, Floquet oscillations in periodically driven dirac systems, *Phys. Rev. B* **101**, 134302 (2020).

[11] N. H. Lindner, G. Refael, and V. Galitski, Floquet topological insulator in semiconductor quantum wells, *Nat. Phys.* **7**, 490 (2011).

[12] A. Gómez-León and G. Platero, Floquet-bloch theory and topology in periodically driven lattices, *Phys. Rev. Lett.* **110**, 200403 (2013).

[13] J. Cayssol, B. Dóra, F. Simon, and R. Moessner, Floquet topological insulators, *Phys. Status Solidi RRL – Rapid Res. Lett.* **7**, 101 (2013).

[14] A. C. Potter, T. Morimoto, and A. Vishwanath, Classification of interacting topological floquet phases in one dimension, *Phys. Rev. X* **6**, 041001 (2016).

[15] A. Eckardt, Colloquium: Atomic quantum gases in periodically driven optical lattices, *Rev. Mod. Phys.* **89**, 011004 (2017).

[16] S. Yao, Z. Yan, and Z. Wang, Topological invariants of floquet systems: General formulation, special properties, and floquet topological defects, *Phys. Rev. B* **96**, 195303 (2017).

[17] T. Oka and S. Kitamura, Floquet engineering of quantum materials, *Annu. Rev. Condens. Matter Phys.* **10**, 387 (2019).

[18] Z. Gong, Y. Ashida, K. Kawabata, K. Takasan, S. Higashikawa, and M. Ueda, Topological phases of non-hermitian systems, *Phys. Rev. X* **8**, 031079 (2018).

[19] H. Zhou and J. Y. Lee, Periodic table for topological bands with non-Hermitian symmetries, *Phys. Rev. B* **99**, 235112 (2019).

[20] K. Kawabata, K. Shiozaki, M. Ueda, and M. Sato, Symmetry and topology in non-hermitian physics, *Phys. Rev. X* **9**, 041015 (2019).

[21] J. C. Budich and E. J. Bergholtz, Non-hermitian topological sensors, *Phys. Rev. Lett.* **125**, 180403 (2020).

[22] E. J. Bergholtz, J. C. Budich, and F. K. Kunst, Exceptional topology of non-Hermitian systems, *Rev. Mod. Phys.* **93**, 015005 (2021).

[23] R. Lin, T. Tai, L. Li, and C. H. Lee, Topological non-Hermitian skin effect, *Front. Phys.* **18**, 10.1007/s11467-023-1309-z (2023).

[24] N. Okuma and M. Sato, Non-hermitian topological phenomena: A review, *Annu. Rev. Condens. Matter Phys.* **14**, 83 (2023).

[25] J. Gong and Q.-h. Wang, Stabilizing non-Hermitian systems by periodic driving, *Phys. Rev. A* **91**, 042135 (2015).

[26] S. Longhi, Floquet exceptional points and chirality in non-Hermitian hamiltonians, *J. Phys. Math. Theor.* **50**, 505201 (2017).

[27] B. Höckendorf, A. Alvermann, and H. Fehske, Topological origin of quantized transport in non-Hermitian floquet chains, *Phys. Rev. Res.* **2**, 023235 (2020).

[28] X. Zhang and J. Gong, Non-hermitian floquet topological phases: Exceptional points, coalescent edge modes, and the skin effect, *Phys. Rev. B* **101**, 045415 (2020).

[29] H. Wu, B.-Q. Wang, and J.-H. An, Floquet second-order topological insulators in non-Hermitian systems, *Phys. Rev. B* **103**, L041115 (2021).

[30] P. Sierant, G. Chiriacò, F. M. Surace, S. Sharma, X. Turkeshi, M. Dalmonte, R. Fazio, and G. Pagano, Dissipative floquet dynamics: From steady state to measurement induced criticality in trapped-ion chains, *Quantum*

tum **6**, 638 (2022).

[31] L. Zhou and D.-J. Zhang, Non-hermitian floquet topological matter—a review, *Entropy* **25**, 10.3390/e25101401 (2023).

[32] F. Koch and J. C. Budich, Dissipative frequency converter: From lindblad dynamics to non-Hermitian topology, *Phys. Rev. Res.* **6**, 033124 (2024).

[33] G. K. Dash, S. Bid, and M. Thakurathi, Floquet exceptional topological insulator, *Phys. Rev. B* **109**, 035418 (2024).

[34] C. C. Wanjura and A. Nunnenkamp, Unifying framework for non-Hermitian and hermitian topology in driven-dissipative systems (2025).

[35] F. Song, S. Yao, and Z. Wang, Non-hermitian skin effect and chiral damping in open quantum systems, *Phys. Rev. Lett.* **123**, 170401 (2019).

[36] F. Minganti, A. Miranowicz, R. W. Chhajlany, I. I. Arkhipov, and F. Nori, Hybrid-liouvillian formalism connecting exceptional points of non-Hermitian hamiltonians and liouvillians via postselection of quantum trajectories, *Phys. Rev. A* **101**, 062112 (2020).

[37] T. Mori, Floquet states in open quantum systems, *Annu. Rev. Condens. Matter Phys.* **14**, 35 (2023).

[38] K. Monkman and M. Berciu, Limits of the lindblad and non-Hermitian description of open systems (2025).

[39] C. M. Dai, Z. C. Shi, and X. X. Yi, Floquet theorem with open systems and its applications, *Phys. Rev. A* **93**, 032121 (2016).

[40] J. C. Budich, Y. Hu, and P. Zoller, Helical floquet channels in 1D lattices, *Phys. Rev. Lett.* **118**, 105302 (2017).

[41] F. Koch and J. C. Budich, Quantum non-Hermitian topological sensors, *Phys. Rev. Res.* **4**, 013113 (2022).

[42] A. Chaduteau, D. K. K. Lee, and F. Schindler, Lindbladian versus postselected non-hermitian topology (2025).

[43] W. Chen, M. Abbasi, S. Erdamar, J. Muldoon, Y. N. Joglekar, and K. W. Murch, Engineering nonequilibrium steady states through floquet liouvillians, *Phys. Rev. Lett.* **134**, 090402 (2025).

[44] C. L. Kane and E. J. Mele, Quantum spin hall effect in graphene, *Phys. Rev. Lett.* **95**, 226801 (2005).

[45] C.-H. Liu, H. Hu, and S. Chen, Symmetry and topological classification of floquet non-Hermitian systems, *Phys. Rev. B* **105**, 214305 (2022).

[46] H. Geng, J. Y. Wei, M. H. Zou, L. Sheng, W. Chen, and D. Y. Xing, Nonreciprocal charge and spin transport induced by non-Hermitian skin effect in mesoscopic heterojunctions, *Phys. Rev. B* **107**, 035306 (2023).

[47] T. E. Lee, Anomalous edge state in a non-hermitian lattice, *Phys. Rev. Lett.* **116**, 133903 (2016).

[48] S. Yao and Z. Wang, Edge states and topological invariants of non-hermitian systems, *Phys. Rev. Lett.* **121**, 086803 (2018).

[49] F. K. Kunst, E. Edvardsson, J. C. Budich, and E. J. Bergholtz, Biorthogonal bulk-boundary correspondence in non-hermitian systems, *Phys. Rev. Lett.* **121**, 026808 (2018).

[50] K. Yokomizo and S. Murakami, Non-bloch band theory of non-hermitian systems, *Phys. Rev. Lett.* **123**, 066404 (2019).

[51] C. H. Lee and R. Thomale, Anatomy of skin modes and topology in non-Hermitian systems, *Phys. Rev. B* **99**, 201103 (2019).

[52] G. Lindblad, On the generators of quantum dynamical semigroups, *Commun. Math. Phys.* **48**, 119 (1976).

[53] V. Gorini, A. Kossakowski, and E. C. G. Sudarshan, Completely positive dynamical semigroups of n-level systems, *J. Math. Phys.* **17**, 821 (1976).

[54] W. Pauli, Zur quantenmechanik des magnetischen elektrons, *Z. Für Phys.* **43**, 601 (1927).

[55] H.-P. Breuer and F. Petruccione, *The Theory of Open Quantum Systems*, 1st ed. (Clarendon Press, Oxford [u.a.], 2009).

[56] C. W. Gardiner and P. Zoller, *Quantum Noise: A Handbook of Markovian and Non-Markovian Quantum Stochastic Methods with Applications to Quantum Optics*, 3rd ed., Springer Complexity (Springer, Berlin, 2010).

[57] Y. Ashida, Z. Gong, and M. Ueda, Non-hermitian physics, *Adv. Phys.* **69**, 249 (2020).

[58] R. B. Griffiths, Consistent interpretation of quantum mechanics using quantum trajectories, *Phys. Rev. Lett.* **70**, 2201 (1993).

[59] H. M. Wiseman, Quantum trajectories and quantum measurement theory, *Quantum Semiclassical Opt. J. Eur. Opt. Soc. Part B* **8**, 205 (1996).

[60] A. J. Daley, Quantum trajectories and open many-body quantum systems, *Adv. Phys.* **63**, 77 (2014).

[61] A. Sergi, The density matrix in the non-Hermitian approach to open quantum system dynamics, *Atti Accad. Peloritana Dei Pericolanti Cl. Sci. Fis. Mat. Nat.* **97**, 11 (2019).

[62] N. Okuma, K. Kawabata, K. Shiozaki, and M. Sato, Topological origin of non-hermitian skin effects, *Phys. Rev. Lett.* **124**, 086801 (2020).

[63] K. Zhang, Z. Yang, and C. Fang, Correspondence between winding numbers and skin modes in non-hermitian systems, *Phys. Rev. Lett.* **125**, 126402 (2020).

[64] R. A. Horn and C. R. Johnson, *Topics in Matrix Analysis* (Cambridge University Press, Cambridge; New York, 1994).

[65] T. Kato, *Perturbation Theory for Linear Operators*, Classics in Mathematics, Vol. 132 (Springer Berlin Heidelberg, Berlin, Heidelberg, 1995).

[66] F. Benaych-Georges and R. R. Nadakuditi, The eigenvalues and eigenvectors of finite, low rank perturbations of large random matrices, *Advances in Mathematics* **227**, 494 (2011).

[67] C. Mehl, V. Mehrmann, A. C. M. Ran, and L. Rodman, Eigenvalue perturbation theory of classes of structured matrices under generic structured rank one perturbations, *Linear Algebra and its Applications Special Issue: Dedication to Pete Stewart on the Occasion of His 70th Birthday*, **435**, 687 (2011).

[68] T. Tao, Outliers in the spectrum of iid matrices with bounded rank perturbations, *Probab. Theory Relat. Fields* **155**, 231 (2013).

[69] C. Bordenave, F. Chapon, and M. Capitaine, *Outliers of perturbations of banded Toeplitz matrices* (2024), arXiv:2410.16439 [math].